Pressure Induced Reduction in $SrUO_4$ – a Topotactic Pathway to Accessing Extreme Incompressibility

Gabriel L. Murphy [a,b,1], Zhaoming Zhang [b,*], Helen E. Maynard-Casely [b], Joshua Stackhouse [c], Piotr M. Kowalski [d,e], Thomas Vogt [f], Evgeny V. Alekseev [g], and Brendan J. Kennedy [a,*]

[a] *School of Chemistry, The University of Sydney, Sydney, NSW 2006, Australia*

[b] *Australian Nuclear Science and Technology Organisation, Lucas Heights, NSW 2234, Australia*

[c] *Department of Nuclear Engineering, University of California, Berkeley, CA 94708, USA*

[d] *Institute of Energy and Climate Research (IEK-13), Forschungszentrum Jülich GmbH, 52428 Jülich, Germany*

[e] *Jülich Aachen Research Alliance, JARA Energy & Center for Simulation and Data Science (CSD), 52425 Jülich, Germany*

[f] *NanoCenter and Department of Chemistry & Biochemistry, University of South Carolina, SC 29208, USA*

[g] *Institute of Energy and Climate Research (IEK-9), Forschungszentrum Jülich GmbH, 52428 Jülich, Germany*

*corresponding authors: Zhaoming Zhang (zhaoming.zhang@ansto.gov.au) and Brendan J. Kennedy (Brendan.Kennedy@Sydney.edu.au)

[1] Present address: *Institute of Energy and Climate Research (IEK-6), Forschungszentrum Jülich GmbH, 52428 Jülich, Germany*

Keywords: Uranium oxide; Neutron diffraction; Ab initio calculations; Lattice defects; Bonding

Abstract:

A combined experimental and theoretical investigation is presented which examines the compressibility of two $SrUO_{4-x}$ polymorphs, α and β, under hydrostatic conditions and explains contrasting chemical and mechanical behaviours in terms of differences in oxygen defect formation chemistry. Via Rietveld refinements against *in situ* neutron powder diffraction measurements, the uranyl bonds in the α-$SrUO_4$ and β-$SrUO_4$ are shown to expand by approximately 20% when subjected to hydrostatic pressures of up to 6 GPa. This is consistent with a reduction of the uranium formal oxidation state from +6 towards +4. Supported by *ab initio* calculations using density functional theory, the origin of the reduction is ascribed to the development of oxygen vacancies leading to the formation of $SrUO_{4-x}$ phases. Remarkably, very different apparent bulk moduli, 591(100) and 60(3) GPa, were found for α-$SrUO_{4-x}$ and β-$SrUO_{4-x}$ respectively, which are attributed to the difference in the preferred lattice sites for oxygen defect formation. In α-$SrUO_{4-x}$ oxygen vacancies preferentially form at the in-plane equatorial sites of the UO_8 polyhedra rather than the uranyl sites leading to enhanced electrostatic interlayer repulsion effects with increasing pressure. In contrast, the formation of oxygen vacancies in β-$SrUO_{4-x}$ form at energetically favourable uranyl sites of the UO_6 polyhedra, which negates the electrostatic repulsion and therefore is more conducive to compression.

1. Introduction

Uranium oxides form the keystone of the nuclear fuel cycle where knowledge of their performance, particularly under extreme pressure and temperature conditions, is imperative to

their safe usage and final disposal. The nature of chemical bonding in uranium oxides has attracted prolonged focus due to its demonstrated influence on the performance of nuclear power reactors and on the severity of accidents [1-4]. Chemical pressure by appropriate substitution and subjecting a material to high pressure are effective pathways to probe chemical bonding and have advanced our understanding in a variety of compounds [5-7]. Although chemical substitution has been commonly used in uranium oxides, high-pressure experimentation is rarely used due to the limited number of facilities capable of conducting such experiments involving radioactive materials [8]. This has led researchers to use theoretical and computational methods to probe the impact of pressure on the bonding in uranium as well as other actinide oxides. However, the spatial extent of the 5*f* orbitals, relativistic effects and the competition between localisation and delocalisation of the orbitals, present significant challenges in the fundamental understanding of bonding derived from computational methods [9-11]. With the progressive transition away from fossil fuels the spotlight is once again on nuclear energy as an alternative to address intermittency challenges within the current infrastructure [12]. This is driving a surge in experimental studies of chemical bonding in uranium oxides with a focus to support its safe use, storage and disposal.

The bonding properties of the ubiquitous linear uranyl ($[O=U=O]^{m+}$) moiety, with bond order three, that occurs in U+6 and U+5 but not U+4 compounds, have been extensively studied [13, 14]. The uranyl moiety combines with other equatorial ligands to form various UO_2L_n polyhedra with L= O, Cl, F and n being predominantly 4 and 6. In the compound UO_2F_2 six equatorial fluorine ligands combine with the uranyl group to form $[UO_2F_6]^{n-}$ anions [15, 16], whereas $[UO_2Cl_4]^{n-}$ anions in $Cs_2UO_2Cl_4$ consist of four equatorial chlorine atoms in a plane perpendicular to the axial linear uranyl groups [17]. The oxo-bonding nature of the uranyl group has been shown to dictate the structural dimensionality and bulk properties of many uranyl oxides as illustrated by the negative linear compressibility of $UO_2(C_2O_4)\cdot H_2O$ [18].

Reorientation of the uranyl pentagonal bipyramids was found to be at the origin of this peculiar phenomena [18]. Osman and co-workers [17] suggested, using density functional theory (DFT), that at pressures below 10 GPa the strong uranyl bonds in $Cs_2UO_2Cl_4$ would weaken and therefore the U-O distance would increase. This peculiar effect was attributed to electron charge transfer from the Cl ligands into the uranyl antibonding orbitals, resulting in an increase of the U-O distances. Warzecha and co-workers [19], using the quantum theory of atoms in molecules (QTAIM) approach with complete active space self-consistent field (CASSCF) wave functions supported by Raman spectroscopic measurements, argued that this was not the correct model for the bonding in $Cs_2UO_2Cl_4$. In contrast to Osman *et al.*'s DFT analysis, their calculations show that the uranyl U-O bonds receive less charge from the U-Cl bonds and therefore the uranyl U-O bond would strengthen and hence shorten under pressure. The difference in the two modeling approaches is an overestimation of the covalence of the U-Cl bonds in the DFT calculations. The stronger covalence of the U-O bonds compared to the U-Cl bonds would suggest that charge transfer in $[UO_6]^{n-}$ or $[UO_8]^{n-}$ anions from the 4 or 6 equatorial U-O bonds could be sufficient to result in a weakening, and subsequent expansion of the uranyl U-O bonds in uranium oxides like $SrUO_4$ as predicted by Osman and co-workers' DFT calculations.

$SrUO_4$ can be prepared in either a rhombohedral (α-$SrUO_4$) or orthorhombic (β-$SrUO_4$) polymorph depending on the synthesis conditions, the former requiring reducing atmosphere [20-22]. The α-$SrUO_4$ structure consists of edge sharing UO_8 polyhedra that form rigid 2D layers, with their shorter collinear axial oxygen atoms, the uranyl groups, pointing perpendicular to the neighbouring planes containing the Sr^{+2} cations, which are also eight-coordinated by oxygen. The structure of α-$SrUO_4$ is depicted in Figure 1a. The structure of β-$SrUO_4$ also contains collinear axial oxygen atoms and consists of corner sharing UO_6 polyhedra forming perforated 2D layers (Figure 1b). The uranyl groups in β-$SrUO_4$ also point towards

the planes containing the Sr^{+2} cations. However, they are slightly tilted compared to the motif in α-$SrUO_4$. Previously Matar and Demazeau [23] calculated that the arrangement of the uranyl groups in $CaUO_4$, which is isostructural to α-$SrUO_4$ [20], are aligned normal to the rigid [UO_8] layers, producing a large bulk moduli under anisotropic compression. α-$SrUO_4$ and isostructural $CaUO_4$ undergo a remarkable reversible phase transformation under reducing conditions at high temperatures, associated with an ordering of oxygen defects leading to the lowering of the crystallographic symmetry [24, 25]. The importance of oxygen defects has also been illustrated in recent investigations of several binary uranium oxides [26, 27]. In this paper we have studied the compressibility of α-$SrUO_4$ and β-$SrUO_4$, possessing $[UO_8]^{n-}$ and $[UO_6]^{n-}$ motifs respectively, under pressure using both *in situ* neutron powder diffraction (NPD), as well as utilising the DFT-based parameter free DFT+*U* method.

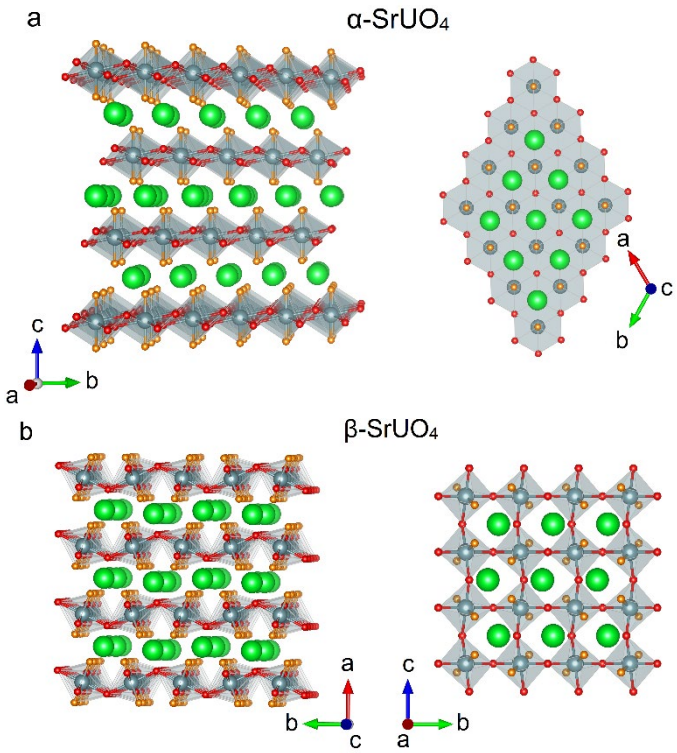

Figure 1. Representations of the crystal structures of (a) rhombohedral α-$SrUO_4$ in space group $R\bar{3}m$, and (b) orthorhombic β-$SrUO_4$ in space group *Pbcm*. Silver, green, red and orange spheres represent uranium, strontium, equatorial oxygen and uranyl oxygen atoms,

respectively. Note that the α-$SrUO_4$ structural models in (a) were drawn in the hexagonal setting for clarity.

2. Experimental and Simulation Details

Single phase samples of $SrUO_4$ were obtained from previous investigations [20, 24, 28], where their synthesis was described [20]. The structures were confirmed by Rietveld refinements using the program GSAS [29, 30] against neutron powder diffraction (NPD) data measured on the Echidna diffractometer [31, 32] at the Australian Centre for Neutron Scattering, part of the Australian Nuclear Science and Technology Organisation (ANSTO).

2.1. High Pressure in situ Neutron Powder Diffraction

The $SrUO_4$ polymorphs were mixed with lead metal, used as an internal pressure standard, and a small amount of deuterated 4:1 ethanol-methanol mixture which acted as the pressure transmitting medium. The resulting slurries were loaded into TiZr encapsulated gaskets [33], which were placed in a VX-5 Paris-Edinburgh hydraulic press equipped with boron nitride anvils [34]. The samples were pre-compressed prior to transport to the neutron beamline, to ensure containment of the radioactive material. Neutron powder diffraction (NPD) data were acquired using the high intensity neutron diffractometer Wombat [35] at ANSTO's Australian Centre for Neutron Scattering where the pressure was determined from the diffraction patterns of lead [36]. High-pressure neutron diffraction measurements were conducted using the 'small' Ge 335 monochromator, which affords better resolution than the more regularly used focusing Ge 113 monochromator. Specifically, the 224 reflection was used resulting in a neutron wavelength of 1.63 Å. α-$SrUO_4$ and β-$SrUO_4$ were pressed incrementally towards maximum load pressures of 1200 and 1000 bar respectively. Using the diffraction from the lead standard these load pressures were determined to correspond to maximum pressures

of 6.16(5) and 5.715(70) GPa respectively on the samples [36]. Refinements were performed using GSAS [29, 30] with the Rietveld refinement method [37]. The peak shapes were modelled using a pseudo-Voigt function, and the background was estimated by a 12-term shifted Chebyshev function. The scale factor, detector zero-point, lattice parameters, atomic coordinates and atomic displacement parameters were refined together with the peak profile parameters. EosFit-7c [38] using the EosFit GUI [39] was applied to determine the equation of state (EoS) for α-$SrUO_4$ and β-$SrUO_4$, respectively, using the refined unit cell volumes from the NPD data.

2.2. Ab Initio Calculations

The *ab initio* simulations were performed with the DFT plane wave Quantum-ESPRESSO package [40] using the setup successfully applied in our previous studies of AUO_4 compounds [24, 25, 28, 41]. In order to investigate the structural changes in $SrUO_4$ compounds we specifically applied the PBEsol exchange-correlation functional [42], which improves the description of structural data over other commonly used functionals, *e.g.*, PBE [42]. We applied the plane-wave energy cutoff of 70 Ryd and the core electrons were modelled by scalar relativistic ultrasoft presuopotentials [43]. All the calculations were spin polarised with the ferromagnetic arrangement of the spins obtained as the minimum energy states for all the magnetic, oxygen deficient compounds. We note, however, that the magnetic arrangement (except U^{+6} that has a non-magnetic $6s^26p^65f^06d^07s^0$ ground state) does not have significant effect on the computed structures or the energies with the energy difference between FM and AFM states smaller than 10 kJ/mol. The final configurations were tested using the occupation matrix control (OMC), as described by Dorado and co-workers [44], as applied in our previous studies [45, 46]. We computed supercells containing 8 and 4 formula units for α and β phases respectively, applying the Methfessel−Paxton 2x2x2 and 4x3x3 k-point grids [47]. The use of

supercells was necessary to estimate the defect formation energies. Atomic configurations and lattice parameters of all the structures were optimised to the equilibrium values at the given applied pressure. The strong correlations between *f* electrons were taken into account with a self-consistent DFT+*U* scheme [48, 49], in which we derived the strength of the Coulomb on-site interaction using the linear response method [48]. All calculations were spin polarised and the spin configurations were carefully checked to achieve the ground state electronic configurations of the considered systems [45, 49]. Such an approach was successfully applied in various previous studies, including those on $SrUO_4$ compounds (*e.g.*, [24, 28]). In order to understand the volume effect on the extend of the structural distortion especially the uranyl bond, we computed the structures of the considered compounds at different pressures, ranging from 0 to 10 GPa.

2.3. Bond Valence Sums calculations

Bond valence sums (BVS) calculations were undertaken using values from Burns and co-workers [50] for U and Brese and O'Keeffe [51] for Sr and associated experimentally determined bond lengths from α-$SrUO_4$ and β-$SrUO_4$.

3. Results

3.1. Pressure Dependence of the Bond Lengths

The pressure dependence of the U-O distances in both $SrUO_4$ polymorphs, from Rietveld refinements using NPD measurements, up to ~6 GPa is shown in Figure 2, along with values at 0 and 5 GPa from *ab initio* calculations using the DFT+*U* method with different oxidation states of uranium (see section 3.3 for details). The refined uranyl U-O distances at ambient pressure are in good agreement with those previously established by high resolution NPD [20]. Although there are two crystallographically distinct equatorial distances of U-O(2)

and U-O(3) in β-$SrUO_4$, for clarity we have plotted their average distance to represent the equatorial U-O length.

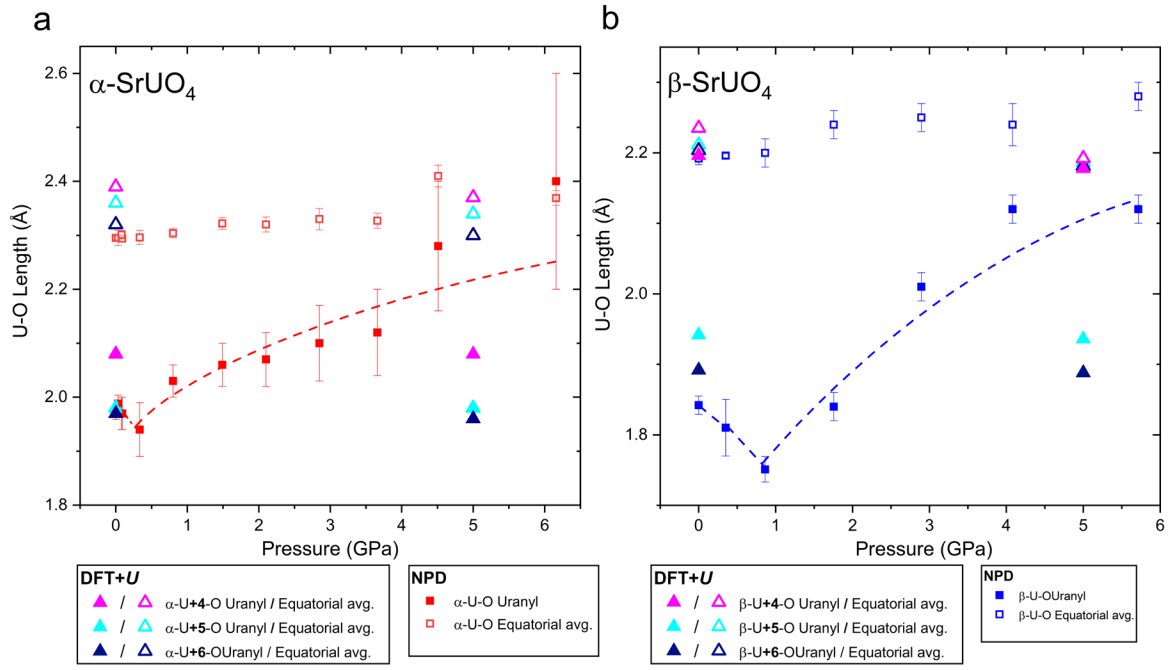

Figure 2. Pressure dependence of the U-O bond lengths in (a) α-$SrUO_4$ (red squares) and (b) β-$SrUO_4$ (blue squares) obtained from neutron diffraction data, and values at 0 and 5 GPa from *ab initio* calculations using DFT+*U* with different oxidation states of uranium in +4, +5 and +6 (triangles). The dashed lines are a guide to the eye and illustrate the initial decrease and subsequent increase in the uranyl U-O distances (closed symbols) with increasing pressures. Note that the sudden jump in the uranyl U-O value of α-$SrUO_4$ between the pressure of 3.7 and 4.5 GPa is believed to be associated with the decreasing crystallinity of the sample, and the dashed line has been drawn to reflect that.

Up to near 0.5 and 1 GPa, for α-$SrUO_4$ and β-$SrUO_4$ respectively, contraction of the uranyl U-O bonds is observed whereas the equatorial U-O bonds largely resist compression. Remarkably, above these pressures a significant expansion of the uranyl U-O bonds is observed in both polymorphs. At the highest pressure, the uranyl bonds in α-$SrUO_4$ and β-$SrUO_4$ have

expanded by a considerable 22% to 2.4(2) Å at 6.16(5) GPa and 15% to 2.12(2) Å at 5.72(7) GPa, respectively, when compared to their distances at ambient pressure (see Supplementary Information Tables S1 and S2 for details). A possible explanation for the observed increase of the uranyl U-O bond distances is that it is a result of a pressure-induced charge transfer from the equatorial ligands to the uranyl entity. This was suggested in the DFT calculations of $Cs_2UO_2Cl_4$ by Osman and co-workers which resulted in a minor increase of the uranyl bond length of approximately 0.3% [17]. The average equatorial bond lengths have also increased moderately by 3% and 4% for α-$SrUO_4$ and β-$SrUO_4$ respectively. The U-O distances we observe are not typical for a uranyl motif where the U is in the +6 oxidation state [52, 53] but are instead more consistent with those observed for U in the +5 oxidation state ($U\text{-}O_{avg}$ = 2.145 Å, for $CrUO_4$ [54]) and in U+4 oxides ($U\text{-}O_{avg}$ = 2.368 Å, for UO_2 [55]), particularly in the case of α-$SrUO_4$. The average Sr-O bond distances have also decreased significantly by approximately 8% in both polymorphs over the studied pressure range.

Previous experimental investigations of perovskite oxides have shown that pressure induced changes to bond valence sums (BVS) of two metal cations can be used as a proxy to monitor changes to bonding environments under pressure, provided the system remains closed [56-58]. Extending this concept to the $SrUO_4$ polymorphs indicates that near 6 GPa the U in both $SrUO_4$ polymorphs has undergone a significant reduction in their BVS values by approximately 2 valence units, whereas the Sr cations have conversely increased their BVS by nearly 2 valence units to a chemically implausible value (see Supplementary Information Figure S4a). In the structurally related $SrMoO_4$ and $SrWO_4$ compounds, Errandonea *et al*. [59] reported that at pressures towards 10 GPa, the average Sr-O bond-length contracts by approximately 3% in both cases. This corresponds to an increase of the BVS value of the Sr cations by 0.5 and 0.7 valence units for $SrMoO_4$ and $SrWO_4$ respectively and is considerably lower than the increase of approximately 2 valence units for Sr observed here in the $SrUO_4$

polymorphs over a smaller pressure range. Such a significant increase in the BVS of the Sr site, primarily due to the O(1) bond valence contribution (Supplementary Information Figures S4b and S4c), implies the occurrence of significant electrostatic interactions. The BVS of the O(1) (uranyl) site shows a distinct shift in contribution from U to Sr upon compression in both polymorphs, coinciding with the onset of bond elongation. The increase in the U-O(1) distance is indicative of the removal of electron density from the uranyl bond, suggestive of an increase in the ionic character. The formation of O(1) (uranyl) vacancy defects would counteract the unrealistic increase of the Sr BVS with increasing pressure [60].

3.2. Pressure Dependence of the Unit Cell Volume

The pressure dependence of the normalised unit cell volume derived from Rietveld refinements against NPD patterns of the two $SrUO_4$ polymorphs is presented in Figure 3. It is evident, when comparing the pressure-volume trend for the $SrUO_4$ polymorphs, that β-$SrUO_4$ is considerably more compressible than α-$SrUO_4$. For both polymorphs several EoS models were tested to describe the pressure-volume trend, including Murnaghan, Birch-Murnaghan and Vinet, and are detailed in the Supplementary Information (Figure S5) [61]. For β-$SrUO_4$, a 3rd order Murnaghan equation of state (EoS) model [62] resulted in the best fitting factor with an apparent bulk modulus of 60(3) GPa. For α-$SrUO_4$, the goodness of fit is essentially model independent, hence a 3rd order Murnaghan EoS was also used to describe its pressure volume trend, yielding a very high apparent bulk modulus of 591(100) GPa. Details of the EoS analysis can be found in the Supplementary Information (Tables S4 and S5). The fitting of the 3rd order Murnaghan to α-$SrUO_4$ resulted in large uncertainties, due to the low-pressure range and the small changes of the unit cell volume of α-$SrUO_4$. This is further impacted by the decrease of crystallinity of the sample under pressure which results in diffraction peaks with large peak width as can be seen in Figures S2 and S3 in the Supplementary Information

(including the diffraction pattern obtained upon the release of pressure at the end of the experiment, confirming that the samples have not decomposed during the high pressure experiment). Nevertheless, when comparing the pressure-volume trend in Figure 3 it is immediately apparent that β-$SrUO_4$ is considerably more compressible than α-$SrUO_4$. For further comparison, data from hydrostatic compression of diamond and its associated Vinet EoS by Occelli *et al*. [63] are plotted in Figure 3. When comparing the normalised unit cell data of α-$SrUO_4$ with diamond, it is evident that over the studied pressure range it exhibits a comparable incompressibility to diamond, although the origin and mechanism of these are very different as discussed below. The presence of the uranyl moiety with U+4 is unexpected due to the known incompatibility between this oxidation state and the bonding type [13, 14]. Furthermore, the reduction of U+6 cannot be realised without the presence of significant oxygen defects since oxidation states higher than Sr^{+2} are not realistic.

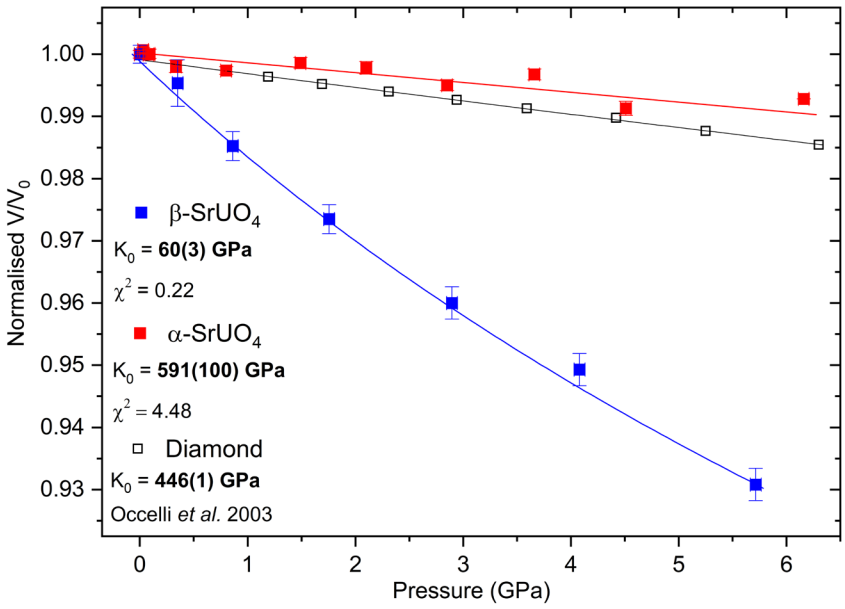

Figure 3. Pressure dependence of the normalised unit cell volume for α-$SrUO_4$ (red markers) and β-$SrUO_4$ (blue markers) obtained from neutron diffraction data (where not apparent the errors are smaller than the symbols). The red and blue lines correspond to a 3rd order

Murnaghan [62] EoS for α-$SrUO_4$ and β-$SrUO_4$. For comparison the black markers show hydrostatic compression of diamond by Occelli *et al.* [63].

3.3. Ab Initio Calculations and Structural Analysis

Although differences in the oxygen defect formation between the two polymorphs have been previously established under ambient pressure conditions [20, 24, 25, 28], the impact of pressure was not considered. Consequently, *ab initio* calculations, using DFT-based parameter free DFT+*U* method with the Hubbard *U* parameter (*U* = 2.5 eV) derived from the linear response theory [24, 28, 48], were undertaken to understand the energetics of possible reduced uranium states and bond elongation under pressure. In these calculations the structures were fully relaxed. The first question to address through simulations was the pressure induced structural changes in the two $SrUO_4$ phases, particularly the stark relative difference in the measured compressibility. Assuming no stoichiometric changes (*i.e.*, without the formation of oxygen vacancy defects), the pressure dependence of the volume and uranyl bond lengths in both polymorphs of $SrUO_4$ was calculated to be as expected for oxides, *i.e.*, there was no expansion in the bond lengths with pressure nor was there extreme incompressibility (see Figure 4). Consequently, it was concluded that hydrostatic pressure exerted on the stoichiometric line compounds does not account for the extraordinary changes in volume or bond expansion, seen experimentally. The BVS calculations (Supplementary Information Figure S4) suggest that bond elongation promotes the formation of U+4. To corroborate this, we computed the structures of both $SrUO_4$ polymorphs with U+5 and U+4, by enforcing a magnetisation of 1 and 2 respectively on the uranium atoms, at 0 and 5 GPa. The calculated uranyl and equatorial bond lengths at 0 and 5 GPa for both polymorphs are plotted in Figures 2a and 2b along with the experimental values as a function of pressure. The calculated uranyl bond lengths and structure energies at 5 GPa are also given in Table 1 with comparative values

from NPD experiments. It is evident from Table 1 that the calculated uranyl bond length of β-$SrUO_4$ at 5 GPa is most consistent with the NPD experiment when the uranium oxidation state is +4, *i.e.*, the pressure induced bond elongation is consistent with a reduction of the U from +6 towards +4 in β-$SrUO_4$, as suggested by the BVS calculations. The agreement between the calculated and experimental results for α-$SrUO_4$ is not as good with the calculated change of 0.12 Å being noticeably less than that experimentally observed, however the experimental uncertainties at the higher pressures are larger due to the decrease in crystallinity.

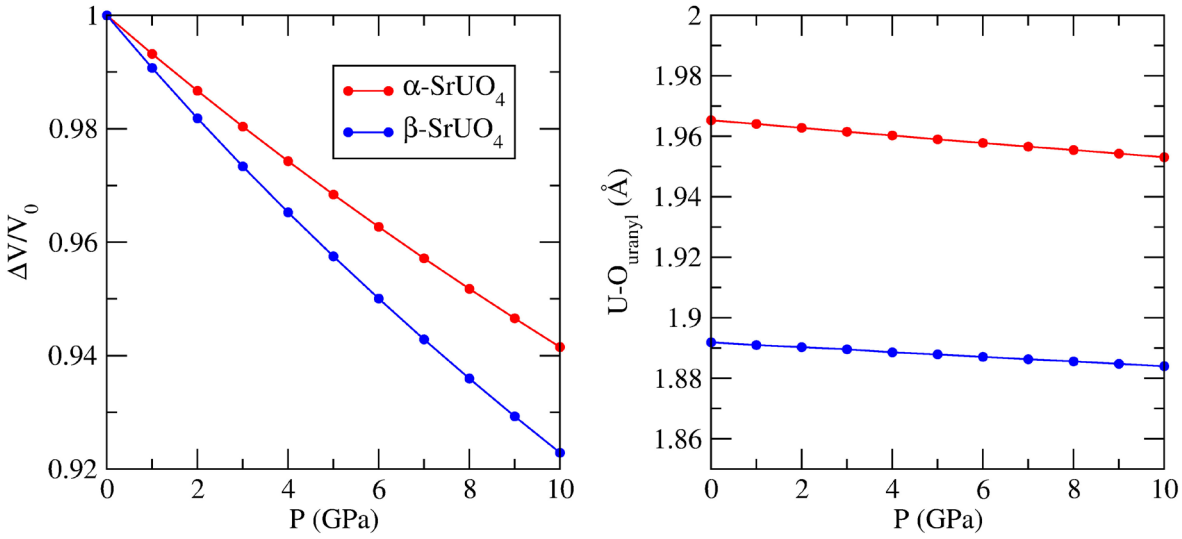

Figure 4. The simulated change in volume and uranyl U-O bond length for α-$SrUO_4$ (red) and β-$SrUO_4$ (blue) when compressed hydrostatically, assuming no oxygen vacancy formation. These calculations assume that the anion sites are fully occupied in both structures during compression. EoS models were fitted against the simulated volumes of α-$SrUO_4$ and β-$SrUO_4$ with calculated bulk moduli found to be 147.21(22) GPa and 105.22(05) GPa, respectively.

Table 1. The uranyl bond lengths in both $SrUO_4$ structures computed with enforced U+6, U+5 and U+4. Computations were performed assuming a pressure of 5 GPa. The internal energy of the resulting structures is reported taking U+6 as a reference. NPD experimentally derived uranyl bond lengths from Rietveld refinements for β-$SrUO_4$ at 0 and 5.72 GPa and α-$SrUO_4$ at 0 and 4.51 GPa are also given.

α-$SrUO_4$	**U-O uranyl (Å)**	**Energy (kJ/mol)**	**Ionic radius (Å) [64]**
U+6	1.96	0	0.73
U+5	1.98	170	0.76
U+4	2.08	433	0.89
α-$SrUO_4$ at 0 GPa	1.970(11)	-	-
α-$SrUO_4$ at 4.51 GPa	2.28(12)	-	-
β-$SrUO_4$	**U-O uranyl (Å)**	**Energy (kJ/mol)**	**Ionic radius (Å) [64]**
U+6	1.89	0	0.73
U+5	1.94	196	0.76
U+4	2.18	472	0.89
β-$SrUO_4$ at 0 GPa	1.842(13)	-	-
β-$SrUO_4$ at 5.72 GPa	2.12(2)	-	-

The presence of U+4 / U+5 in either $SrUO_4$ polymorph is not possible without introducing oxygen vacancy defects at either the uranyl oxygen or in-plane oxygen positions. From our previous studies on oxygen defect formation energy in the two $SrUO_4$ polymorphs at ambient pressure [24], we know that the formation of such a structure would cost ~250-350 kJ/mol [25]. The BVS calculations (see Supplementary Information Figure S4) show that the pressure induced increase in the strontium BVS to an unrealistic +4 oxidation state is a result of primarily the uranyl oxygen atoms moving towards the strontium cation. The formation of vacancies at the uranyl site has the potential to negate this influence. In Table 2 we present the

oxygen defect formation energies, the energies of forming the four $SrUO_3$-type structures derived from the two $SrUO_4$ polymorphs. In these calculations the topology of the structures was retained and neutral oxygen defects were computed. We note that charged defects with charges between 2- and 2+ were also computed with the procedure of Crocombette *et al*. [65], and the corresponding defect formation energies were found to be at least 100 kJ/mol higher.

Table 2. Oxygen defect formation energies, the U-O distances, and the energies of forming four potential $SrUO_3$-type structures derived from $SrUO_4$ topotactically (by removing oxygens from either in-plane or uranyl positions respectively).

	α-$SrUO_4$	β-$SrUO_4$
O-def uranyl defect formation energy (kJ/mol)	**418**	**339**
U-O distance (uranyl) (Å)	2.12	2.26
'$SrUO_3$' formation energy (kJ/mol)	324	303
O-def in plane defect formation energy (kJ/mol)	**206**	**455**
U-O distance (in plane) (Å)	2.04	2.22
'$SrUO_3$' formation energy (kJ/mol)	292	301

Table 2 shows that the formation of defects under the experimental conditions is within the expected range of their energies. An important distinction between the two polymorphs is the difference between the energy required to induce defects on the uranyl site compared to the in-plane equatorial position. In β-$SrUO_4$, it is more energetically favourable for vacancies to occur on the uranyl-oxygen site than the in-plane position, with a difference in energy of -116 kJ/mol (difference between the two energies in bold in Table 2). Conversely, defects are far less favourable on the uranyl site than the in-plane equatorial site in α-$SrUO_4$ where the difference in the defect formation energy is +212 kJ/mol. We note that the formation of oxygen defects in either phase is accompanied by the formation of a pair of U+5 species for an in-plane defect and the formation of a single U+4 for a uranyl defect. The over bonding of the Sr (hinted

by the unrealistically high BVS of the Sr) is avoided if the oxygen defects occur on the uranyl site. This is favourable for β-$SrUO_4$ but not for α-$SrUO_4$. We suggest that the inability to form defects on the uranyl oxygen site in α-$SrUO_4$ leads to its large apparent incompressibility, as the internal electrostatic repulsion caused by the strengthening interaction of the uranyl oxygen with the Sr cation upon bond contraction cannot be energetically alleviated through the defect formation, as in β-$SrUO_4$. This is clearly visible when comparing the unit cell volumes of the respective $SrUO_4$ and '$SrUO_3$' phases (see Supplementary Information Table S3), the latter derived from topotactically removing oxygens from either in-plane (α-$SrUO_4$) or uranyl (β-$SrUO_4$) positions. For the α structure-type the unit cell volume of the fully reduced α-$SrUO_3$ species at 5 GPa is larger than that of α-$SrUO_4$ at 0 GPa. While for the β structure-type the opposite is observed, with the β-$SrUO_3$ species at 5 GPa having the smaller unit cell volume than that of β-$SrUO_4$ at 0 GPa. Here we use the labels of α-$SrUO_3$ and β-$SrUO_3$ to indicate that these structures are derived from their corresponding $SrUO_4$ polymorph. The broadening of the Bragg reflections with increasing pressure, evident in Supplementary Information Figure S2 and S3, is consistent with a decrease in long-range ordering, which is expected to occur if appreciable numbers of vacancies formed in the lattice. These figures also illustrate the difference in the compression of the Pb internal marker and $SrUO_4$. Uranium oxides have been found to be active as oxidation catalysts where the oxygen atoms originate from the lattice facilitate the uranium redox couple and predisposition of oxides such as U_3O_8 to oxygen non-stoichiometry [66, 67].

4. Discussion

The observed structural changes and DFT calculations strongly indicate that a significant number of oxygen defects form in both $SrUO_4$ polymorphs upon the application of pressure. A striking feature of the pressure response of the uranyl U-O distances displayed in

Figure 2 is the minima at pressures near 0.5 and 1 GPa, for α-$SrUO_4$ and β-$SrUO_4$, respectively. Modest pressures, above these minima, cause the formation of oxygen defects which results in a charge transfer impacting the uranyl character of the axial U-O groups and the associated reduction of the uranium oxidation state from +6 towards +4. This is comparable to that suggested for $Cs_2UO_2Cl_4$ by Osman and co-workers [17]. Whilst similar in nature, they reported a small increase in the uranyl bond distance of 0.006 Å to roughly 10 GPa, whereas we observed an increase of 0.43 Å to 6.2 GPa that is almost two orders of magnitude larger. The observed lengthening of the axial U-O bonds corresponds to a loss of their "uranyl" character. At the same time the Sr-O bonds contract and become more ionic. That this process is pressure dependent implies that reduced oxidation states of U can be accessed and controlled through the application of pressure in uranium oxides.

An important observation is the remarkably different compressibility between α-$SrUO_{4-x}$ and β-$SrUO_{4-x}$. *Ab initio* calculations show that in the absence of defects the compression behaviour of the two stoichiometric polymorphs is similar (see Figure 4). The bulk modulus in metals, covalent materials, and partly in ionic compounds, is primarily determined by the density of valence electrons. For many ionic compounds the bulk modulus $B \sim 1/V \sim \rho$, where V is the specific volume [68], and for covalent materials with a diamond-like structure $B \sim 1/d^{3.5} \sim \rho^{1.17}$, where d is the interatomic distance [69]. The intrinsic compressibility of a material is therefore determined primarily by the spatially averaged electron density. The large bulk modulus in the case of diamond is a result of its high electron (and atomic) density, which is due to its small ionic radius and four valence electrons coupled with its three-dimensionally bound sp^3 carbon atom. However, the behaviours of α-$SrUO_{4-x}$ and β-$SrUO_{4-x}$ under pressure are due to a distinctly different mechanism than found in diamond (which is an intrinsic effect), namely the formation of oxygen defects during compression resulting in a topotactic structural change. Non-stoichiometry is observed in many materials where the underlying topology of

the material is unaltered. The bulk mechanical properties are usually determined by the topology but can be altered by the change in stoichiometry. Defect formation does not usually result in enhanced incompressibility, as illustrated in the computational study of hyperstoichiometric UO_{2+x}. As described by Wang *et al*. [70] the addition of defects (interstitial oxygen) in cubic fluorite structured UO_{2+x} decreases the bulk modulus. Conversely the same change in defect concentration in the orthorhombic structured cotunnite polymorph results in a small increase in the bulk modulus. Similar softening of materials with defects has been recently described in experimental studies of defect and non-defect containing ABX_3 perovskites and Prussian Blue analogues [71, 72]. In α-$SrUO_4$ the apparent incompressibility stems from its topology and bond lengthening of the uranyl bond, and energetics of oxygen defect formation. In β-$SrUO_4$ the uranyl groups are tilted away from the Sr-containing layers whereas in α-$SrUO_4$ they are aligned normal to the Sr-containing layers (Figure 5). This leads to stronger initial electrostatic repulsions in α-$SrUO_4$ compared to β-$SrUO_4$. The pressure induced charge transfer and the resulting elongation of the uranyl groups further amplifies this difference in electrostatic repulsion as corroborated by the BVS calculations. The effects of increased hydrostatic pressure and electrostatic repulsion can be reduced by the formation of oxygen defects in the uranyl moieties and by forming defect $SrUO_{4-x}$ structures. As shown by DFT calculations this is energetically favourable in β-$SrUO_{4-x}$, but not in α-$SrUO_{4-x}$ where, consequently, large incompressibility resists any further increase of electrostatic repulsion. This results in a situation for α-$SrUO_{4-x}$ in which the resistance for uranyl oxygen defects to occur is balanced against the increasingly repulsive electrostatic interactions between the expanding uranyl bonds and the Sr cations. Consequently, when the experimentally established compressive behaviours of the two $SrUO_{4-x}$ polymorphs are compared to the intrinsic behaviours predicted in the absence of any defects as determined using DFT (Figure 4), β-$SrUO_{4-x}$ is observed to be slightly more compressive, whereas α-$SrUO_{4-x}$ is significantly more

incompressible. This impact of defects is consistent with the recent studies of Bostrom *et al.* [71, 72] referred to above. Evidently the competing interactions and unfavourable energetic process in α-$SrUO_{4-x}$ during compression result in extreme incompressibility that is comparable to the intrinsic hardness of diamond. Direct comparison between the intrinsic bulk modulus of diamond with the measured, or extrinsic, bulk modulus of α-$SrUO_{4-x}$ is somewhat hypothetical due to the pressure dependent formation of defects in the latter. By realising different extrinsic states in the two polymorphs of $SrUO_4$, the compressibility can be dramatically altered. The formation of defects at the axial (uranyl) sites in β-$SrUO_{4-x}$ results in softening whereas in α-$SrUO_{4-x}$ the defects occur at the equatorial sites producing an apparent bulk modulus comparable to that of diamond.

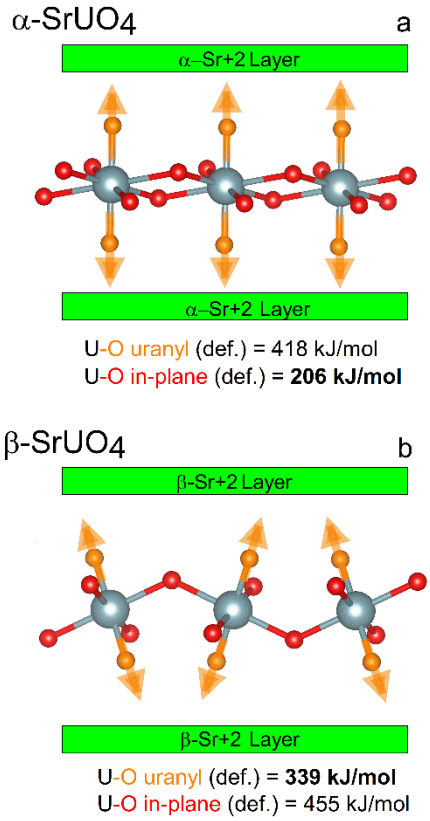

Figure 5. Graphical representations of the different orientation of the uranyl groups in (a) α-$SrUO_4$ and (b) β-$SrUO_4$ respectively, along with the oxygen defect formation energies at the uranyl and in-plane positions.

DFT calculations show that the formation of oxygen defects at the in-plane equatorial positions is energetically more likely in α-$SrUO_4$ whereas defects at the uranyl positions are favoured in β-$SrUO_4$. In α-$SrUO_4$ with its rigid [UO_8] layers and uranyl groups aligned normal to the Sr-containing layers, bond elongation results in very unfavourable electrostatic repulsions that cannot be alleviated due to its inability to form oxygen defects in the uranyl groups. Consequently, as pressure and axial U-O bond length increase, the electrostatic repulsion between the uranyl groups and the Sr cations also grows and this creates a mechanical resistance to further expansion resulting in a large incompressibility and an apparent bulk modulus akin to diamond. Conversely in β-$SrUO_4$ the uranyl groups are tilted away from the Sr-containing layers and the formation of oxygen vacancy defects at the uranyl sites reduces the unfavourable bonding of the Sr cation enabling further compression of the unit cell. Prior to this study there were no reports of uranium compounds undergoing a topotactic pressure-induced charge transfer reaction, resulting in the reduction of uranium and lengthening of the uranyl bonds. This work has unveiled the unexpected pressure-induced reduction of uranium and the formation of oxygen defects at modest pressures resulting in extreme incompressibility in α-$SrUO_4$ and points to the possibility of realising and utilising extrinsic factors such as defects to make new ultrahard materials from appropriate 'precursor materials'. Furthermore, this is a cautionary tale that assuming the persistence of a line compound when exploring physical properties of materials under pressure might not always be justified. Instead, radically different properties might result from a subtle non-stoichiometry created under pressure.

5. Conclusion

Using *in-situ* high-pressure neutron powder diffraction, supported by *ab initio* DFT calculations, we establish that the preferential expansion of the uranyl bonds in both α-$SrUO_4$

and β-$SrUO_4$ with increasing pressure is caused by significant oxygen defect formation and subsequent reduction of U with oxidation state +6 towards +4. The orientation of the uranyl bond and relative difference in the energy required to induce oxygen defect formation in the uranyl and in-plane oxygen positions impact the measured compressibility of α - and β-$SrUO_4$. Fits of the measured volume-pressure data, using the 3rd order Murnaghan EoS model, indicate that the α-form has a significantly higher apparent bulk modulus, 591(100) GPa, compared to 60(3) GPa of the β-form. This value for α-$SrUO_4$ is remarkably high, in fact it is comparable to the intrinsic bulk modulus of diamond at 446(1) GPa [63]. Our calculation of the intrinsic bulk modulus of defect free α-$SrUO_4$ via the DFT+*U* method results in a considerably lower value of 147.21(22) GPa which is consistent with the literature DFT value of 132 GPa [73]. This huge discrepancy between the apparent and computed intrinsic bulk moduli supports our interpretation that topotactic oxygen defect formation enhances the incompressibility which is not considered in the computational analysis of stoichiometric α-$SrUO_4$. It should be emphasised that the creation of oxygen vacancies alters the stoichiometry from α-$SrUO_4$ to non-stoichiometric α-$SrUO_{4-x}$, consequently the observed incompressibility does not correspond to the intrinsic bulk modulus. Nevertheless, this work demonstrates that by utilising extrinsic properties, such as defect phenomena, extreme diamond-like incompressibility can be obtained with potential for practical applications.

Acknowledgements

This work was, in part, performed at the Australian Centre for Neutron Scattering (proposal #6016). We acknowledge the support of the Australian Research Council and the Australian Institute of Nuclear Science and Engineering. GLM acknowledges and greatly appreciates the support and encouragement from Dr Chris Griffith, Dr Robert Gee and ANSTO Minerals with radioactive materials handling, laboratory usage and continual support for this

research. The calculations were performed with the computational resources of Forschungszentrum Jülich and RWTH Aachen awarded for the project on the JARA-CSD.

References

[1] P.C. Burns, R.C. Ewing, A. Navrotsky, Nuclear fuel in a reactor accident, Science 335(6073) (2012) 1184-1188.
[2] L.B. Skinner, C.J. Benmore, J.K.R. Weber, M.A. Williamson, A. Tamalonis, A. Hebden, T. Wiencek, O.L.G. Alderman, M. Guthrie, L. Leibowitz, J.B. Parise, Molten uranium dioxide structure and dynamics, Science 346(6212) (2014) 984-987.
[3] M.W.D. Cooper, C.R. Stanek, D.A. Andersson, The role of dopant charge state on defect chemistry and grain growth of doped UO_2, Acta Materialia 150 (2018) 403-413.
[4] C. Onofri, C. Sabathier, C. Baumier, C. Bachelet, D. Drouan, M. Gérardin, M. Legros, Extended defect change in UO_2 during in situ TEM annealing, Acta Materialia 196 (2020) 240-251.
[5] S.A.J. Kimber, A. Kreyssig, Y.-Z. Zhang, H.O. Jeschke, R. Valentí, F. Yokaichiya, E. Colombier, J. Yan, T.C. Hansen, T. Chatterji, R.J. McQueeney, P.C. Canfield, A.I. Goldman, D.N. Argyriou, Similarities between structural distortions under pressure and chemical doping in superconducting $BaFe_2As_2$, Nature Materials 8(6) (2009) 471-475.
[6] J. Wang, F. Zhang, J. Lian, R.C. Ewing, U. Becker, Energetics and concentration of defects in $Gd_2Ti_2O_7$ and $Gd_2Zr_2O_7$ pyrochlore at high pressure, Acta Materialia 59(4) (2011) 1607-1618.
[7] Y. Wang, R. Hrubiak, S. Turczyński, D.A. Pawlak, M. Malinowski, D. Włodarczyk, K.M. Kosyl, W. Paszkowicz, H. Przybylińska, A. Wittlin, A. Kaminska, Y. Zhydachevskyy, M.G. Brik, L. Li, C.-G. Ma, A. Suchocki, Spectroscopic properties and martensitic phase transition of $Y_4Al_2O_9$:Ce single crystals under high pressure, Acta Materialia 165 (2019) 346-361.
[8] K. O'Nions, R. Pitman, C. Marsh, Science of nuclear warheads, Nature 415(6874) (2002) 853-857.
[9] I. Fryer-Kanssen, A. Kerridge, Elucidation of the inverse trans influence in uranyl and its imido and carbene analogues via quantum chemical simulation, Chemical Communications 54(70) (2018) 9761-9764.
[10] J. Su, E.R. Batista, K.S. Boland, S.E. Bone, J.A. Bradley, S.K. Cary, D.L. Clark, S.D. Conradson, A.S. Ditter, N. Kaltsoyannis, J.M. Keith, A. Kerridge, S.A. Kozimor, M.W. Loble, R.L. Martin, S.G. Minasian, V. Mocko, H.S. La Pierre, G.T. Seidler, D.K. Shuh, M.P. Wilkerson, L.E. Wolfsberg, P. Yang, Energy-degeneracy-driven covalency in actinide bonding, Journal of the American Chemical Society 140(51) (2018) 17977-17984.
[11] S.C. Middleburgh, W.E. Lee, M.J.D. Rushton, Structure and properties of amorphous uranium dioxide, Acta Materialia 202 (2021) 366-375.
[12] C.D. Ferguson, L.E. Marburger, J.D. Farmer, A. Makhijani, A US nuclear future?, Nature 467(7314) (2010) 391-393.
[13] M.L. Neidig, D.L. Clark, R.L. Martin, Covalency in f-element complexes, Coordination Chemistry Reviews 257(2) (2013) 394-406.
[14] V. Vallet, U. Wahlgren, I. Grenthe, Probing the nature of chemical bonding in uranyl(VI) complexes with quantum chemical methods, The Journal of Physical Chemistry A 116(50) (2012) 12373-12380.
[15] M. Atoji, M.J. McDermott, Crystal structure of anhydrous UO_2F_2, Acta Crystallographica Section B 26(OCT15) (1970) 1540-1544.
[16] S.F. Matar, Electronic structure and chemical bonding properties of UO_2F_2 from first principles, Solid State Sciences 11(8) (2009) 1380-1385.

[17] H.H. Osman, P. Pertierra, M.A. Salvado, F. Izquierdo-Ruiz, J.M. Recio, Structure and bonding in crystalline cesium uranyl tetrachloride under pressure, Phys. Chem. Chem. Phys. 18(27) (2016) 18398-18405.
[18] F. Colmenero, J. Cobos, V. Timón, Negative linear compressibility in uranyl squarate monohydrate, Journal of Physics: Condensed Matter 31(17) (2019) 175701.
[19] E. Warzecha, C. Celis-Barros, T. Dilbeck, K. Hanson, T.E. Albrecht-Schmitt, High-pressure studies of cesium uranyl chloride, Inorg. Chem. 58(1) (2019) 228-233.
[20] G. Murphy, B.J. Kennedy, B. Johannessen, J.A. Kimpton, M. Avdeev, C.S. Griffith, G.J. Thorogood, Z.M. Zhang, Structural studies of the rhombohedral and orthorhombic monouranates: $CaUO_4$, α-$SrUO_4$, β-$SrUO_4$ and $BaUO_4$, J. Solid State Chem. 237 (2016) 86-92.
[21] T. Fujino, N. Masaki, H. Tagawa, The crystal structures of alpha-$SrUO_4$ and gamma-$SrUO_4$, Z. Kristall. 145(3-4) (1977) 299-309.
[22] B.O. Loopstra, H.M. Rietveld, Structure of some alkaline-earth metal uranates, Acta Crystallographica Section B 25 (1969) 787-791.
[23] S.F. Matar, G. Demazeau, Electronic band structure of $CaUO_4$ from first principles, J. Solid State Chem. 182(10) (2009) 2678-2684.
[24] G.L. Murphy, C.H. Wang, G. Beridze, Z.M. Zhang, J.A. Kimpton, M. Avdeev, P.M. Kowalski, B.J. Kennedy, Unexpected crystallographic phase transformation in nonstoichiometric $SrUO_{4-x}$: reversible oxygen defect ordering and symmetry lowering with increasing temperature, Inorg. Chem. 57(10) (2018) 5948-5958.
[25] G.L. Murphy, C.H. Wang, Z.M. Zhang, P.M. Kowalski, G. Beridze, M. Avdeev, O. Muransky, H.E.A. Brand, Q.F. Gu, B.J. Kennedy, Controlling oxygen defect formation and its effect on reversible symmetry lowering and disorder-to-order phase transformations in nonstoichiometric ternary uranium oxides, Inorg. Chem. 58(9) (2019) 6143-6154.
[26] Y. Li, A fundamental understanding of the structures of oxygen defect clusters in UO_{2+x}, U_4O_9 and U_3O_7: from the perspective of Tetris cubes, Acta Materialia 194 (2020) 482-495.
[27] T.R. Pavlov, M.R. Wenman, L. Vlahovic, D. Robba, R.J.M. Konings, P. Van Uffelen, R.W. Grimes, Measurement and interpretation of the thermo-physical properties of UO_2 at high temperatures: The viral effect of oxygen defects, Acta Materialia 139 (2017) 138-154.
[28] G.L. Murphy, B.J. Kennedy, J.A. Kimpton, Q.F. Gu, B. Johannessen, G. Beridze, P.M. Kowalski, D. Bosbach, M. Avdeev, Z.M. Zhang, Nonstoichiometry in strontium uanium oxde: understanding the rhombohedral-orthorhombic transition in $SrUO_4$, Inorg. Chem. 55(18) (2016) 9329-9334.
[29] A.C. Larson, R.B. Von Dreele, General Structure Analysis System (GSAS), Los Alamos National Laboratory Report LAUR 86-748, 2004.
[30] B.H. Toby, EXPGUI, a graphical user interface for GSAS, J. Appl. Cryst. 34 (2001) 210-213.
[31] M. Avdeev, J.R. Hester, ECHIDNA: a decade of high-resolution neutron powder diffraction at OPAL, Journal of Applied Crystallography 51(6) (2018) 1597-1604.
[32] K.-D. Liss, B. Hunter, M. Hagen, T. Noakes, S. Kennedy, Echidna - the new high-resolution powder diffractometer being built at OPAL, Physica B 385-86 (2006) 1010-1012.
[33] W.G. Marshall, D.J. Francis, Attainment of near-hydrostatic compression conditions using the Paris-Edinburgh cell, Journal of Applied Crystallography 35 (2002) 122-125.
[34] J. Besson, R. Nelmes, G. Hamel, J. Loveday, G. Weill, S. Hull, Neutron powder diffraction above 10 GPa, Physica B: Condensed Matter 180 (1992) 907-910.
[35] A.J. Studer, M.E. Hagen, T.J. Noakes, Wombat: The high-intensity powder diffractometer at the OPAL reactor, Physica B: Condensed Matter 385 (2006) 1013-1015.
[36] T. Strässle, S. Klotz, K. Kunc, V. Pomjakushin, J.S. White, Equation of state of lead from high-pressure neutron diffraction up to 8.9 GPa and its implication for the NaCl pressure scale, Physical Review B 90(1) (2014) 014101.
[37] H.M. Rietveld, A profile refinement method for nuclear and magnetic structures, Journal of Applied Crystallography 2(2) (1969) 65-71.

[38] R.J. Angel, M. Alvaro, J. Gonzalez-Platas, EosFit7c and a Fortran module (library) for equation of state calculations, Zeitschrift für Kristallographie - Crystalline Materials 229(5) (2014) 405-419.
[39] J. Gonzalez-Platas, M. Alvaro, F. Nestola, R. Angel, EosFit7-GUI: a new graphical user interface for equation of state calculations, analyses and teaching, Journal of Applied Crystallography 49(4) (2016) 1377-1382.
[40] P. Giannozzi, S. Baroni, N. Bonini, M. Calandra, R. Car, C. Cavazzoni, D. Ceresoli, G.L. Chiarotti, M. Cococcioni, I. Dabo, QUANTUM ESPRESSO: a modular and open-source software project for quantum simulations of materials, Journal of physics: Condensed matter 21(39) (2009) 395502.
[41] G.L. Murphy, Z. Zhang, R. Tesch, P.M. Kowalski, M. Avdeev, E.Y. Kuo, D.J. Gregg, P. Kegler, E.V. Alekseev, B.J. Kennedy, Tilting and distortion in rutile-related mixed metal ternary uranium oxides: A structural, spectroscopic, and theoretical investigation, Inorg. Chem. 60(4) (2021) 2246-2260.
[42] J.P. Perdew, A. Ruzsinszky, G.I. Csonka, O.A. Vydrov, G.E. Scuseria, L.A. Constantin, X. Zhou, K. Burke, Restoring the density-gradient expansion for exchange in solids and surfaces, Physical review letters 100(13) (2008) 136406.
[43] D. Vanderbilt, Soft self-consistent pseudopotentials in a generalized eigenvalue formalism, Physical review B 41(11) (1990) 7892-7895.
[44] B. Dorado, B. Amadon, M. Freyss, M. Bertolus, DFT+*U* calculations of the ground state and metastable states of uranium dioxide, Physical Review B 79(23) (2009) 235125.
[45] K.O. Kvashnina, P.M. Kowalski, S.M. Butorin, G. Leinders, J. Pakarinen, R. Bès, H. Li, M. Verwerft, Trends in the valence band electronic structures of mixed uranium oxides, Chemical Communications 54(70) (2018) 9757-9760.
[46] M. Sun, J. Stackhouse, P.M. Kowalski, The +2 oxidation state of Cr incorporated into the crystal lattice of UO_2, Communications Materials 1(1) (2020) 13.
[47] M. Methfessel, A.T. Paxton, High-precision sampling for brillouin-zone integration in metals, Physical Review B 40(6) (1989) 3616-3621.
[48] M. Cococcioni, S. De Gironcoli, Linear response approach to the calculation of the effective interaction parameters in the LDA+ *U* method, Physical Review B 71(3) (2005) 035105.
[49] G. Beridze, P.M. Kowalski, Benchmarking the DFT+ *U* method for thermochemical calculations of uranium molecular compounds and solids, The Journal of Physical Chemistry A 118(50) (2014) 11797-11810.
[50] P.C. Burns, R.C. Ewing, F.C. Hawthorne, The crystal chemistry of hexavalent uranium: Polyhedron geometries, bond-valence parameters, and polymerization of polyhedra, Canadian Mineralogist 35 (1997) 1551-1570.
[51] N.E. Brese, M. O'Keeffe, Bond-valence parameters for solids, Acta Crystallographica Section B 47(2) (1991) 192-197.
[52] P.C. Burns, U^{6+} minerals and inorganic compounds: Insights into an expanded structural hierarchy of crystal structures, Canadian Mineralogist 43 (2005) 1839-1894.
[53] A.J. Lussier, R.A. Lopez, P.C. Burns, A revised and expanded structure hierarchy of natural and synthetic hexavalent uranium compounds, The Canadian Mineralogist 54(1) (2016) 177-283.
[54] X.F. Guo, E. Tiferet, L. Qi, J.M. Solomon, A. Lanzirotti, M. Newville, M.H. Engelhard, R.K. Kukkadapu, D. Wu, E.S. Ilton, M. Asta, S.R. Sutton, H.W. Xu, A. Navrotsky, U(V) in metal uranates: a combined experimental and theoretical study of $MgUO_4$, $CrUO_4$, and $FeUO_4$, Dalton Trans. 45(11) (2016) 4622-4632.
[55] L. Desgranges, G. Baldinozzi, G. Rousseau, J.-C. Nièpce, G. Calvarin, Neutron diffraction study of the in situ oxidation of UO_2, Inorg. Chem. 48(16) (2009) 7585-7592.
[56] M. Guennou, P. Bouvier, B. Krikler, J. Kreisel, R. Haumont, G. Garbarino, High-pressure investigation of $CaTiO_3$ up to 60 GPa using x-ray diffraction and Raman spectroscopy, Physical Review B 82(13) (2010) 134101.
[57] J. Zhao, N.L. Ross, R.J. Angel, New view of the high-pressure behaviour of $GdFeO_3$-type perovskites, Acta Crystallographica Section B 60(3) (2004) 263-271.

[58] J. Zhao, N.L. Ross, R.J. Angel, Estimation of polyhedral compressibilities and structural evolution of $GdFeO_3$-type perovskites at high pressures, Acta Crystallographica Section B 62(3) (2006) 431-439.
[59] D. Errandonea, R.S. Kumar, X. Ma, C. Tu, High-pressure X-ray diffraction study of $SrMoO_4$ and pressure-induced structural changes, J. Solid State Chem. 181(2) (2008) 355-364.
[60] M.O.J.Y. Hunault, D. Menut, O. Tougait, Alkali uranyl borates: bond length, equatorial coordination and 5f states, Crystals 11(1) (2021) 56.
[61] R.J. Angel, Equations of state, Reviews in Mineralogy and Geochemistry 41(1) (2000) 35-59.
[62] F. Murnaghan, The compressibility of media under extreme pressures, Proceedings of the national academy of sciences of the United States of America 30(9) (1944) 244.
[63] F. Occelli, P. Loubeyre, R. LeToullec, Properties of diamond under hydrostatic pressures up to 140 GPa, Nature Materials 2(3) (2003) 151-154.
[64] R.D. Shannon, Revised effective ionic-radii and systematic studies of interatomic distances in halides and chalcogenides, Acta Crystallographica Section A 32(SEP1) (1976) 751-767.
[65] J.-P. Crocombette, D. Torumba, A. Chartier, Charge states of point defects in uranium oxide calculated with a local hybrid functional for correlated electrons, Physical Review B 83(18) (2011) 184107.
[66] C.S. Heneghan, G.J. Hutchings, S.R. O'Leary, S.H. Taylor, V.J. Boyd, I.D. Hudson, A temporal analysis of products study of the mechanism of VOC catalytic oxidation using uranium oxide catalysts, Catalysis Today 54(1) (1999) 3-12.
[67] G.J. Hutchings, C.S. Heneghan, I.D. Hudson, S.H. Taylor, Uranium-oxide-based catalysts for the destruction of volatile chloro-organic compounds, Nature 384(6607) (1996) 341-343.
[68] O.L. Anderson, J.E. Nafe, The bulk modulus-volume relationship for oxide compounds and related geophysical problems, Journal of Geophysical Research (1896-1977) 70(16) (1965) 3951-3963.
[69] M.L. Cohen, Calculation of bulk moduli of diamond and zinc-blende solids, Physical Review B 32(12) (1985) 7988.
[70] J. Wang, R.C. Ewing, U. Becker, Electronic structure and stability of hyperstoichiometric UO_{2+x} under pressure, Physical Review B 88(2) (2013) 024109.
[71] H.L.B. Boström, I.E. Collings, D. Daisenberger, C.J. Ridley, N.P. Funnell, A.B. Cairns, Probing the influence of defects, hydration, and composition on Prussian blue analogues with pressure, Journal of the American Chemical Society 143(9) (2021) 3544-3554.
[72] H.L.B. Boström, G. Kieslich, Influence of metal defects on the mechanical properties of ABX_3 perovskite-type metal-formate frameworks, The Journal of Physical Chemistry C 125(2) (2021) 1467-1471.
[73] Materials Data on $SrUO_4$ (SG:166), mp-36329, The Materials Project, United States, 2014. doi: 10.17188/1207164.